Turk J Phys
34 (2010) , 123 – 138.

doi:10.3906/fiz-1004-31

# Vibration spectra of polar mixing optical phonon states and Fröhlich electron-phonon coupling behaviors in a wurtzite ZnO quantum dot

**Li ZHANG**
*Department of Mechanism and Electronics, Guangzhou Panyu Polytechnic, Panyu, 511483, People's Republic of CHINA*
*e-mail: zhangli-gz@263.net*

Received 27.04.2010

**Abstract**

Based on the dielectric continuum model and Loudon's uniaxial crystal model, the interface-optical-propagating (IO-PR) mixing phonon states of a quasi-zero-dimensional (Q0D) wurtzite cylindrical quantum dot (QD) are investigated. It is found that there are two types of IO-PR mixing phonon modes, i.e. $\rho$-IO/$z$-PR mixing modes and the $z$-IO/$\rho$-PR mixing modes coexisting in Q0D wurtzite QDs. Numerical calculation on a wurtzite ZnO QD shows that the dispersion frequencies of the mixing modes are discrete functions of the azimuthal quantum number and axial wave-number. The calculated results agree well with the recent experimental spectra in ZnO QDs. An abnormal electron-phonon coupling strength is observed with the increase of the azimuthal quantum number and the order of phonon modes, which is attributed to the modulation effect of anisotropic dielectric functions of wurtzite ZnO crystal. The analytical Frölich-like Hamiltonian of electron-phonon interaction obtained here is quite useful for further analyzing phonon influence on optoelectronics properties of wurtzite Q0D QD structures. The present results can be reduced naturally to those of wurtzite quantum wires or quantum wells as the height or radius of cylindrical QD approaches infinity. This supports the validity and unity of phonon modes theories in wurtzite low-dimensional quantum systems.

**Key Words:** Wurtzite ZnO QDs, phonon states, electron-phonon interactions
**PACS:** 78.67.Hc; 68.35.Ja; 63.20.D-; 63.20.Kd.

## 1. Introduction

Currently, there has been a great deal of interest in investigations of zinc oxide (ZnO) semiconductors [1, 2], which mainly can be concluded into the following four unique features and advantages of ZnO materials: wide direct bandgap ($\sim$3.3 eV at 300 K) that has huge potential for electronic, optoelectronic and optical applications; semiconducting, piezoelectric and pyroelectric properties which result in ZnO being an ideal candidate for fabricating electromechanical coupling devices; biodegradable and possibly biocompatible characteristics

that is suitable for medical and biological applications; various nanostructures, such as dots, wires and belts as well as nanoring, etc., easily formed by a chemical approach or physical method, which leads to a potentially lower cost for ZnO-based devices and equipment. In addition, semiconductor quantum dots (QDs) are nanostructures where the three-dimensional confinement of carriers results in a discrete energy spectrum [3, 4, 5], which can further improve the performance of optoelectronic devices, such as low-threshold lasers and light polarization insensitive detectors. Meanwhile, with the technique advancements in crystal growing, such as metal-organic chemical vapor deposition, the molecular-beam epitaxy and hydride vapor phase epitaxy, ZnO QDs can be fabricated in experiments [5, 6, 7, 8], and it provides explicit and important research object of ZnO nanostructures. Hence investigation of various physical properties in ZnO QD structures has become a hot topic both in theories and experiments during the last decade [1–8].

Though bound electronic states, donor and acceptor impurity states, excitonic states, as well as electron spin dynamics in the quasi-0-dimensional (Q0D) ZnO QD have been widely investigated [7, 8, 9, 10, 11], the polar optical phonon states and their coupling properties with electrons in the system have not been fully understood. The phenomena of phonon replicas in the emission spectra, the homogeneous broadening of excitonic line width and the relaxations of hot carriers to the fundamental band edge are directly relative to the lattice vibration of semiconductor materials [12]. Theories and experiments reveal that not only the carriers, but also the lattice vibrations (phonon modes) are influenced greatly by the heterostructures of low-dimensional quantum systems [13, 14, 15]. Moreover, phonon modes have quite important influence on the optoelectronics and electronics properties of low-dimensional quantum structures [16, 17, 18, 19]. Hence it is necessary to study the phonon modes in ZnO QD structures.

It is well known that ZnO materials usually crystallize in the hexagonal wurtzite structure, whose physical properties behavior anisotropic in space. In contrast to the zinc-blende GaAs-based confined structures [15, 20, 21, 22, 23], the phonon modes in wurtzite quasi-2-dimensional (Q2D) quantum well (QW) and quasi-1-dimensional (Q1D) quantum wire (QWR) systems are more complicated [24, 25, 26, 27, 28, 29, 30, 31, 32]. Due to the complexity of phonon modes in the wurtzite QD structures originated from the high confined dimensionality and anisotropic wurtzite crystal-structure, the optical phonon modes in the ZnO QDs have rarely been studied and not fully been understood [33, 34, 35, 36, 37, 38, 39]. Rajalakshmi et al. [33] and Lin et al. [34] experimentally studied the properties of optical phonon confinement in ZnO QDs by using the Raman spectroscopy, and an obviously confined behavior of optical phonon modes was observed. Based on a dielectric continuum model (DCM) and Raman spectrometry technique, Chassaing and cooperators [35] analyzed theoretically and experimentally the surface optical (SO) phonon modes of a ZnO QDs. In fact, an infinite height QWR and an infinite radius quantum disk (also QW) were assumed in their theoretical analysis. The same group also investigated the acoustic phonons in ZnO nanoparticles, in addition to the usual breathing and fundamental extensional modes, a new extensional mode of ZnO nanoparticles was found [36]. Based on the x-ray absorption, photoluminescence and Raman spectroscopy technique, the groups of Cheng [37] and Hsu [38] studied the size-effect on the properties of electron-longitudinal-optical (LO)-phonon and exciton-LO phonon interactions in wurtzite ZnO QDs. The two groups drew the similar conclusion that the strengths of the electron (exciton)-phonon coupling increase as the sizes of ZnO QD increase. Fonoberov et al. [39] investigated interface optical (IO) and confined optical phonons in wurtzite spherical ZnO QDs. Recently, we [40] extended the works of polar optical phonon modes to the wurtzite nitride cylindrical QDs structures based on the DCM and Loudon's uniaxial crystal model [41]. However, up to now, the polar optical phonon modes in wurtzite cylindrical ZnO QD structures have not been fully studied and understood. Moreover, the geometrical shapes

and symmetries of realistic QDs maybe spherical-caps, spheroids, hexagonal pyramids and cylindroid structures [4, 5, 6, 7, 8, 35, 37, 39], which strongly depend on material natures and growing conditions. For simplicity, we investigate the polar optical phonon modes in a cylindrical ZnO QDs in the present paper.

The main accomplishments and significance of this work can be summarized into four points as follows. (i) The dispersive equation and the Fröhlich-like electron-phonon interaction Hamiltonian for one type of important optical phonon modes, i.e. the IO-propagating (PR) phonon mixing modes in wurtzite QDs are given. The analytical results obtained here are quite useful for further analyzing the phonon dispersion spectra [35] and polaronic effect [15, 16, 17, 18, 19] in the Q0D wurtzite QD structures. (ii) Numerical calculation on a wurtzite ZnO QD is performed. It is found that the dispersion frequencies of the mixing phonon modes are discrete functions of the azimuthal quantum number and axial wave-number of the cylindrical QD systems, and the calculated results agree well with the recent experimental observation [35]. (iii) Via the numerical discussion of the electron-phonon coupling functions, an abnormal electron-phonon coupling strength is observed, which is attributed to the modulation effect of anisotropic dielectric functions in wurtzite ZnO crystal. (iv) The present theoretical results can be reduced naturally to those of wurtzite Q1D QWRs [19, 29, 30] (Q2D QWs [24, 25, 26, 27, 28]) as the height (radius) of the cylindrical QD approaches infinity. This further supports the validity and unity of phonon modes theories in wurtzite low-dimensional quantum systems.

## 2. Theory

Let us consider a freestanding wurtzite cylindrical QD structure with radius $R$ and height $2d$ along the $z$-direction. The $z$-axis is taken to be along the direction of the $c$-axis of the wurtzite material and denote the radial- (axial-) direction as $t$ ($z$). Thus, under the cylindrical coordinate, the heterointerfaces of the wurtzite QD in $z$-direction are located at $z = \pm d$, and in radius-heterointerface is at $\rho = R$. Via solving the Laplace equation based on Loudon's uniaxial crystal model [41], it can be confirmed that there are four types of polar mixing phonon modes in wurtzite cylindrical QD structures [40]. As the first step of solving the complicated mixing optical phonon modes in wurtzite QDs, we will pay attention to the IO-PR mixing phonon modes only in the next text.

The IO-PR mixing mode is a mode which behaves as IO mode in $t(z)$-direction, and shows as PR mode in $z(t)$-direction. Considering the exchange of $t$- and $z$-directions, it is found that the IO-PR mixing modes also have two forms, i.e. the $z-\mathrm{IO}/\rho-\mathrm{PR}$ and $\rho-\mathrm{IO}/z-\mathrm{PR}$ mixing modes. Under cylindrical coordinates, the electrostatic potential functions of $z-\mathrm{IO}/\rho-\mathrm{PR}$ mixing modes are given by

$$
\begin{aligned}
\Phi_m^{z-\mathrm{IO}/\rho-\mathrm{PR}}(\mathbf{r}) &= e^{\mathrm{i}m\varphi} f^{\mathrm{PR}}(\rho)\phi^{\mathrm{IO}}(z), \\
f^{\mathrm{PR}}(\rho) &= \begin{cases} a_1 J_m(k_{t1}\rho) & \rho \leqslant R \\ a_2 J_m(k_{t2}\rho) + a_3 Y_m(k_{t2}\rho) & \rho > R, \end{cases} \\
\phi^{\mathrm{IO}}(z) &= \begin{cases} \begin{cases} b_1 \exp(k_{z2} z) & z < -d \\ b_2 \sinh(k_{z1} z) & |z| \leqslant d \quad \mathrm{AS} \\ -b_1 \exp(-k_{z2} z) & z > d, \end{cases} \\ \begin{cases} b_1 \exp(k_{z2} z) & z < -d \\ b_2 \cosh(k_{z1} z) & |z| \leqslant d \quad \mathrm{S} \\ b_1 \exp(-k_{z2} z) & z > d. \end{cases} \end{cases}
\end{aligned} \tag{1}
$$

For the $\rho-\mathrm{IO}/z-\mathrm{PR}$ mixing modes, their electrostatic potentials can be written as

$$\begin{aligned}
\Phi_m^{\rho-\mathrm{IO}/z-\mathrm{PR}}(\mathbf{r}) &= e^{\mathrm{i}m\varphi} f^{\mathrm{IO}}(\rho)\phi^{\mathrm{PR}}(z), \\
f^{\mathrm{IO}}(\rho) &= \begin{cases} a_1 I_m(k_{t1}\rho) & \rho \leqslant R \\ a_2 K_m(k_{t2}\rho) & \rho > R, \end{cases} \\
\phi^{\mathrm{PR}}(z) &= \begin{cases} \begin{cases} b_1 \exp(\mathrm{i}k_{z2}z) & z < -d \\ b_2 \sin(k_{z1}z) & |z| \leqslant d \quad \mathrm{AS} \\ -b_1 \exp(\mathrm{i}k_{z2}z) & z > d, \end{cases} \\ \begin{cases} b_1 \exp(\mathrm{i}k_{z2}z) & z < -d \\ b_3 \cos(k_{z1}z) & |z| \leqslant d \quad \mathrm{S} \\ b_1 \exp(\mathrm{i}k_{z2}z) & z > d. \end{cases} \end{cases}
\end{aligned} \tag{2}$$

In equation (1), $J_m(x)$ and $Y_m(x)$ are the Bessel and Neumann functions of $m$-order, respectively. In equation (2), $K_m(x)$ and $I_m(x)$ are the first- and second-kind modified Bessel functions of order $m$, respectively. And $a_i$ and $b_i$ are coupling coefficients of phonon modes determining by additional boundary conditions (BCs). The symbols "AS" and "S" in equations (1) and (2) denote the antisymmetrical solution and symmetrical solution, respectively. This treatment completely satisfies the symmetry demand of the phonon potential in $z$-direction.

According to the relationship of Loudon's uniaxial crystal model [41] and the Laplace equation in the areas of the inner and outer QD [40], the dependent relations of the phonon wave-numbers $k_{uv}$ $(u = t, z; v = 1, 2)$ can be chosen as

$$\begin{aligned}
\sqrt{\epsilon_{ti}(\omega)}k_{ti} \pm \sqrt{\epsilon_{zi}(\omega)}k_{zi} &= 0, \\
\sqrt{\epsilon_{z1}(\omega)}k_{z1} \pm \sqrt{\epsilon_{z2}(\omega)}k_{z2} &= 0,
\end{aligned} \tag{3}$$

where

$$\epsilon_t(\omega) = \epsilon_t^{\infty}\frac{\omega^2 - \omega_{t,L}^2}{\omega^2 - \omega_{t,T}^2}, \epsilon_z(\omega) = \epsilon_z^{\infty}\frac{\omega^2 - \omega_{z,L}^2}{\omega^2 - \omega_{z,T}^2}. \tag{4}$$

Here, $\omega_{z,L}$, $\omega_{z,T}$, $\omega_{t,L}$ and $\omega_{t,T}$ are the zone center characteristic frequencies of $\mathrm{A}_1(\mathrm{LO})$, $\mathrm{A}_1(\mathrm{TO})$, $\mathrm{E}_1(\mathrm{LO})$, and $\mathrm{E}_1(\mathrm{TO})$ modes, respectively. It should be noted that subscripts 1 and 2 in equations (1), (2) and (3) correspond to the ZnO material and vacuum dielectric environment, respectively.

The reasonableness of equation (3) lies in the fact that the present theories in wurtzite Q0D QDs can reduce naturally to the corresponding results of wurtzite Q1D QWR and Q2D QW structures under a certain condition, which will be discussed in detail later.

By using the continuity BCs of the potential functions and the electric displacement vector at the axial interfaces $z = \pm d$ and the radial interface $\rho = R$, one can get the following two equations for the $\rho-\mathrm{IO}/z-\mathrm{PR}$ mixing modes, [29, 31]:

$$k_{z1} = n\pi/2d, \ n = \pm 1, \pm 2, ... \tag{5}$$

and

$$\begin{aligned}
&\epsilon_{t,1}k_{t1}K_m(k_{t2}R)[I_{m-1}(k_{t1}R) + I_{m+1}(k_{t1}R)] \\
&+\epsilon_{t2}k_{t2}I_m(k_{t1}R)[K_{m-1}(k_{t2}R) + K_{m+1}(k_{t2}R)] = 0.
\end{aligned} \tag{6}$$

Connecting equations (3), (5) and (6), the dispersive frequencies of $\rho-\mathrm{IO}/z-\mathrm{PR}$ mixing modes can be worked out. In the same way, via the continuity BCs of the potential functions and the electric displacement vector at the axial interfaces $z = \pm d$ and the radial interface $\rho = R$, one can obtain another two dispersive equations (7) and (8) for the $z-\mathrm{IO}/\rho-\mathrm{PR}$ mixing modes [26, 32]. They are given by

$$k_{z1} = \begin{cases} \arctan\mathrm{h}\sqrt{-\epsilon_{z2}/\epsilon_{z1}}/d, & \mathrm{S} \\ \arctan\mathrm{h}\sqrt{-\epsilon_{z1}/\epsilon_{z2}}/d, & \mathrm{AS} \end{cases} \tag{7}$$

and

$$\begin{aligned} &\{k_{t2}\epsilon_{t,2}J_m(k_{t1}R)[J_{m-1}(k_{t2}R) - J_{m+1}(k_{t2}R)] \\ &+k_{t1}\epsilon_{t,1}J_m(k_{t2}R)[J_{m+1}(k_{t1}R) - J_{m-1}(k_{t1}R)]\}Y_m(k_{t2}L) \\ &-J_m(k_{t2}L)\{k_{t1}\epsilon_{t,1}[J_{m+1}(k_{t1}R) - J_{m-1}(k_{t1}R)]Y_m(k_{t2}R) \\ &+k_{t2}\epsilon_{t,2}[Y_{m+1}(k_{t2}R) - Y_{m-1}(k_{t2}R)]J_m(k_{t1}R)\} = 0. \end{aligned} \tag{8}$$

In the same way, "S" and "AS" in equation (7) also denote the symmetric and antisymmetric $z-\mathrm{IO}/\rho-\mathrm{PR}$ mixing modes. In equation (8), $L$ is the maximum radial size of the nonpolar dielectric environment (in general, $L \gg R$). The dispersive frequencies and properties of the $z-\mathrm{IO}/\rho-\mathrm{PR}$ mixing modes in ZnO QDs can be obtained by solving the equations (7) and (8) numerically.

Next we deduce the expressions of the free phonon field Hamiltonian and electron-phonon interaction Hamiltonian. To this end, we first institute the orthonormality relationships of polarization vector of IO-PR mixing phonon modes. Based on the formula $\mathbf{P} = (1-\epsilon)/4\pi\nabla\Phi(\mathbf{r})$, one can get the polarization vector $\mathbf{P}_m^{\mathrm{IO-PR}}(\mathbf{r})$ of IO-PR mixing phonon modes. For the symmetrical and antisymmetrical $z-\mathrm{IO}/\rho-\mathrm{PR}$ mixing modes, the polarization vectors $\mathbf{P}_m^{z-\mathrm{IO}/\rho-\mathrm{PR}}(\mathbf{r})$ are respectively given by

$$\begin{aligned} \mathbf{P}_{\mathrm{S},m}^{z-\mathrm{IO}/\rho-\mathrm{PR}}(\mathbf{r}) &= \frac{A_0}{4\pi}e^{\mathrm{i}m\varphi}\left\{\frac{1}{2}\Phi_{\mathrm{S}}^{\mathrm{IO}}(z)(1-\epsilon_{t1})k_{t1}[J_{m-1}(k_{t1}\rho) - J_{m+1}(k_{t1}\rho)]\widehat{\rho}\right. \\ &\left. + f^{\mathrm{PR}}(\rho)\Phi_{\mathrm{S}}^{\mathrm{IO}}(z)\frac{\mathrm{i}m}{\rho}(1-\epsilon_{t1})\widehat{\varphi} + f^{\mathrm{PR}}(\rho)k_{z1}(1-\epsilon_{z1})b_2\sinh(k_{z1}z)\widehat{z}\right\}, \end{aligned} \tag{9}$$

and

$$\begin{aligned} \mathbf{P}_{\mathrm{AS},m}^{z-\mathrm{IO}/\rho-\mathrm{PR}}(\mathbf{r}) &= \frac{A_0}{4\pi}e^{\mathrm{i}m\varphi}\left\{\frac{1}{2}\Phi_{\mathrm{AS}}^{\mathrm{IO}}(z)(1-\epsilon_{t1})k_{t1}[J_{m-1}(k_{t1}\rho) - J_{m+1}(k_{t1}\rho)]\widehat{\rho}\right. \\ &\left. + f^{\mathrm{PR}}(\rho)\Phi_{\mathrm{AS}}^{\mathrm{IO}}(z)\frac{\mathrm{i}m}{\rho}(1-\epsilon_{t1})\widehat{\varphi} + f^{\mathrm{PR}}(\rho)k_{z1}(1-\epsilon_{z1})b_2\cosh(k_{z1}z)\widehat{z}\right\}. \end{aligned} \tag{10}$$

For the $\rho-\mathrm{IO}/z-\mathrm{PR}$ mixing modes, the polarization vectors $\mathbf{P}_m^{\rho-\mathrm{IO}/z-\mathrm{PR}}(\mathbf{r})$ of symmetrical and antisymmetrical $\rho-\mathrm{IO}/z-\mathrm{PR}$ modes are unified as

$$\begin{aligned} \mathbf{P}_{\mathrm{S/AS},m}^{\rho-\mathrm{IO}/z-\mathrm{PR}}(\mathbf{r}) &= \frac{A_0}{4\pi}e^{\mathrm{i}m\varphi}K_m(k_{t2}R)\left\{\frac{1}{2}\Phi_{\mathrm{S/AS}}^{\mathrm{PR}}(z)(1-\epsilon_{t1})k_{t1}[I_{m-1}(k_{t1}\rho)\right. \\ &+I_{m+1}(k_{t1}\rho)]\widehat{\rho} + f^{\mathrm{IO}}(\rho)\Phi_{\mathrm{S/AS}}^{\mathrm{PR}}(z)\frac{\mathrm{i}m}{\rho}(1-\epsilon_{t1})\widehat{\varphi} \\ &\left.+f^{\mathrm{IO}}(\rho)k_{z1}(1-\epsilon_{z1})[b_2\cos(k_{z1}z) - b_3\sin(k_{z1}z)]\widehat{z}\right\}. \end{aligned} \tag{11}$$

It should be noted that equations (9)–(11) just give the polarization vectors $\mathbf{P}_m^{\mathrm{IO-PR}}(\mathbf{r})$ within the ZnO QD region, and the polarization outside of the QD is null due to the nonpolar vacuum dielectric matrix ($\epsilon_d = 1$).

By making use of the orthonormality condition of polarization vectors $\mathbf{P}_m^{\mathrm{IO-PR}}(\mathbf{r})$, the normalization constants $A_0$ in equation (3) are obtained:

$$\begin{aligned} |A_0|^2 &= \left\{ \frac{e^{-2k_{z2}d}}{\cosh^2(k_{z1}d)} \int \rho \mathrm{d}\rho \mathrm{d}z \{ \frac{\omega_{pt}^2}{\eta_t}(1-\epsilon_{t1})^2 k_{t1}^2 \cosh^2(k_{z1}z) \right. \\ &\left. \times [J_{m-1}^2(k_{t1}\rho) + J_{m+1}^2(k_{t1}\rho)] + 2\frac{\omega_{pz}^2}{\eta_z}(1-\epsilon_{z1})^2 k_{z1}^2 \sinh^2(k_{z1}z) J_m^2(k_{t1}\rho) \} \right\}^{-1} \end{aligned} \tag{12}$$

for symmetrical $z-\mathrm{IO}/\rho-\mathrm{PR}$ mixing modes,

$$\begin{aligned} |A_0|^2 &= \left\{ \frac{e^{-2k_{z2}d}}{\sinh^2(k_{z1}d)} \int \rho \mathrm{d}\rho \mathrm{d}z \{ \frac{\omega_{pt}^2}{\eta_t}(1-\epsilon_{t1})^2 k_{t1}^2 \sinh^2(k_{z1}z) \right. \\ &\left. \times [J_{m-1}^2(k_{t1}\rho) + J_{m+1}^2(k_{t1}\rho)] + 2\frac{\omega_{pz}^2}{\eta_z}(1-\epsilon_{z1})^2 k_{z1}^2 \cosh^2(k_{z1}z) J_m^2(k_{t1}\rho) \} \right\}^{-1} \end{aligned} \tag{13}$$

for antisymmetrical $z-\mathrm{IO}/\rho-\mathrm{PR}$ mixing modes, and

$$\begin{aligned} |A_0|^2 &= \left\{ K_m^2(k_{t2}R) \int \rho \mathrm{d}\rho \mathrm{d}z \{ |\mathcal{B}_2 \cos(k_{z1}z) + \mathcal{B}_3 \sin(k_{z1}z)|^2 \right. \\ &\times \frac{\omega_{pt}^2}{\eta_t}(1-\epsilon_{t1})^2 k_{t1}^2 [I_{m-1}^2(k_{t1}\rho) + I_{m+1}^2(k_{t1}\rho)] \\ &\left. + 2I_m^2(k_{t1}\rho) \frac{\omega_{pz}^2}{\eta_z}(1-\epsilon_{z1})^2 k_{z1}^2 \, |\mathcal{B}_2 \sin(k_{z1}z) + \mathcal{B}_3 \cos(k_{z1}z)|^2 \} \right\}^{-1} \end{aligned} \tag{14}$$

for the symmetrical and antisymmetrical $\rho-\mathrm{IO}/z-\mathrm{PR}$ mixing phonon modes. "$\eta_{vv}$" in equations (12)–(14) is defined as

$$\eta_{vv}^{1/2} = [1 + \alpha_v n^*(4\pi\omega_{0v}^2/\omega_{pv}^2 - 4\pi\omega_0^2/\omega_{pv}^2)]^{-1}, (\nu = i, j; v = t, z), \tag{15}$$

where $\omega_{pv}$ is the ionic plasma frequency. In equation (14), the coupling coefficients $\mathcal{B}_i$ $(i = 2, 3)$ are defined in the Appendix. In terms of the complete set of orthonormal polarization vector $\mathbf{P}_{v,m}^{\mathrm{IO-PR}}$, we can obtain the free phonon Hamiltonian operators for the IO-PR mixing modes, i.e.

$$H_{\mathrm{IO-PR}} = \sum_{m,k_{z1}} \hbar\omega \left[ b_m^\dagger(k_{z1}) b_m(k_{z1}) + \frac{1}{2} \right]. \tag{16}$$

The symbols $b_m^\dagger(k_{z1})$ and $b_m(k_{z1})$ are $m$-th mode creation and annihilation operators for the IO-PR phonons. They satisfy the commutative rules for bosons.

The interaction Hamiltonian of electron with the IO-PR mixing phonon field is read as $H_{\mathrm{e-IO/PR}} = -e\Phi^{\mathrm{IO-PR}}(\mathbf{r})$. Via expanding $\Phi^{\mathrm{IO-PR}}(\mathbf{r})$ in terms of the normal modes obtained above, and after some trivial

algorithms, we get the electron-phonon interaction Hamiltonian as

$$\begin{aligned} H_{\mathrm{e-IO/PR}} &= -e\sum_{m,k_{z1}}\left(\frac{\hbar}{8\pi\omega}\right)^{1/2}\Phi_m^{\mathrm{IO-PR}}(\mathbf{r})[b_m^{\dagger}(k_{z1})+b_m(k_{z1})] \\ &= -\sum_{m,k_{z1}}\Gamma_{m,k_{z1}}^{\mathrm{IO-PR}}(\rho)\Gamma_{m,k_{z1}}^{\mathrm{IO-PR}}(z)[b_m(k_{z1})\mathrm{e}^{\mathrm{i}m\varphi}+\mathrm{H.c.}], \end{aligned} \tag{17}$$

where $\Gamma_{m,k_{z1}}^{\mathrm{IO-PR}}(\rho)$ and $\Gamma_{m,k_{z1}}^{\mathrm{IO-PR}}(z)$ are the coupling functions defined as

$$\begin{aligned} \Gamma_{m,k_{z1}}^{\mathrm{IO-PR}}(\rho) &= \sqrt{|\mathcal{A}_0|}\left(\frac{\hbar e^2}{\omega}\right)^{1/4} f^{\mathrm{IO,PR}}(\rho), \\ \Gamma_{m,k_{z1}}^{\mathrm{IO-PR}}(z) &= \sqrt{|\mathcal{A}_0|}\left(\frac{\hbar e^2}{\omega}\right)^{1/4} \phi^{\mathrm{IO,PR}}(z), \end{aligned} \tag{18}$$

where the functions $f^{\mathrm{IO,PR}}(\rho)$ and $\phi^{\mathrm{IO,PR}}(z)$ are defined in equations (1) and (2).

## 3. Numerical results and discussion

In order to get a clear picture for the dispersive properties of IO-PR mixing phonon modes and their coupling behaviors with electrons in Q0D wurtzite QD system, a numerical calculation is performed on a wurtzite ZnO cylindrical QD. The height $2d$ and the radius $R$ of the cylindrical QD structure are chosen as $2d = R = 2a_B$, respectively. ($a_B$ is the effective Bohr radius of the wurtzite ZnO bulk material, which is approximately 2.1 nm). The physical parameters of the materials used in our calculation are listed in Table 1.

**Table 1**. Zone-center energies (in $\mathrm{cm}^{-1}$) of polar optical phonons, dielectric constants of wurtzite ZnO material and dielectric matrix [1, 26].

| $\omega_{tT}$ | $\omega_{tL}$ | $\omega_{zT}$ | $\omega_{zL}$ | $\epsilon_{z\infty}$ | $\epsilon_{t\infty}$ | $\epsilon_{z0}$ | $\epsilon_{t0}$ | $\epsilon_d$ |
|---|---|---|---|---|---|---|---|---|
| 380 | 579 | 413 | 591 | 3.78 | 3.7 | 8.91 | 7.77 | 1 |

Let us first investigate the dispersive properties of the IO-PR mixing phonon modes. Figure 1 plots the dispersive frequencies $\omega$ of the $\rho-\mathrm{IO}/z-\mathrm{PR}$ mixing modes as a function of the $z$-direction wave-number $k_{z1}$. The first six azimuthal quantum numbers $m = 0, 1, ..., 5$ are considered in the figure. From the figure, it is found that the frequency range of $\rho-\mathrm{IO}/z-\mathrm{PR}$ mixing modes is within the range of $[\omega_{tT1}, \omega_{zL1}]$, which is consistent with the frequency range analysis of mixing phonon modes in Q0D wurtzite QDs [40]. It is observed that the dispersive frequencies $\omega$ of the $\rho-\mathrm{IO}/z-\mathrm{PR}$ mixing phonon modes are the discrete functions of the wave-number $k_{z1}$, which are quite similar to the energy levels of electronic states in Q0D QD structures. This is the typical feature of confined phonon modes in Q0D QD systems [39, 42], and it is obviously different from the dispersive characteristics of confined phonon modes in wurtzite Q2D QWs [24, 25, 26, 27, 28] and Q1D QWRs structures [29, 30, 31, 32]. In wurtzite Q2D QWs (Q1D QWRs) systems, the dispersive frequencies of confined phonon modes are always continuous functions of the plane (axial) wave-numbers due to their translational symmetry [24, 25, 26, 27, 28, 29, 30, 31, 32]. But for the wurtzite cylindrical QDs, they have no translational

symmetry. Thus the dispersive frequencies of phonon modes in wurtzite cylindrical QDs just take a series of discrete values. Apart from the curves of $m = 0, 1$, each of the other curve has a minimum at a certain $k_{z1}$. With increase of $m$, the dispersions of the IO-PR mixing phonon modes become weaker and weaker. We also notice from Figure 1 that all the interval of adjacent $k_{z1}$ for the $\rho$-IO/$z$-PR mixing phonon modes are equal, which can be fully understood from the dispersion equation (5). As $k_{z1}$ approaches $\infty$, the value 542.8 cm$^{-1}$ is the limiting frequency of the $\rho$-IO/$z$-PR mixing phonon modes. In fact, based on the relations [43]

$$\begin{aligned} \lim_{x\to\infty} I_m(x) &= e^x/\sqrt{2\pi x}, \\ \lim_{x\to\infty} K_m(x) &= e^{-x}\sqrt{\pi}/\sqrt{2x}, \end{aligned} \tag{19}$$

it is easy to prove that, as $k_{z1} \to \infty$, equation (6) will degenerate to the form of $\epsilon_{t1} + 1 = 0$. This equation just gives the limited frequency of 542.8 cm$^{-1}$. These are the general features of phonon modes in low-dimensional quantum structures [24, 25, 26, 27, 28, 29, 30, 31, 32].

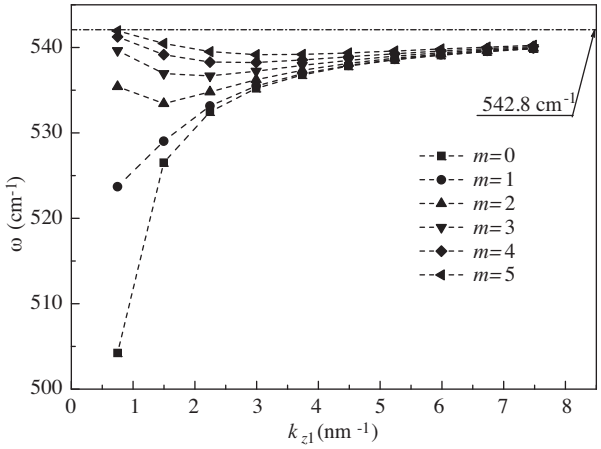


**Figure 1**. Dispersive frequencies $\omega$ of the $\rho-$IO/$z-$PR mixing modes as a function of the $z$-direction wave-number $k_{z1}$ for six different azimuthal quantum numbers $m = 0, 1, 2, ..., 5$.

Figure 2 depicts the dispersive frequencies $\omega$ of $z$-IO/$\rho$-PR mixing phonon modes as a function of $k_{z1}$. Three different azimuthal quantum number $m = 0, 1, 2$ are chosen. It is observed clearly that there are two branches of $z$-IO/$\rho$-PR mixing modes in ZnO cylindrical QDs. The high frequency branch (the upper branch) is the antisymmetrical $z$-IO/$\rho$-PR mixing phonon mode, and the low frequency branch (the nether branch) is the symmetrical $z$-IO/$\rho$-PR mixing mode. The first dot ($n = 1$) of the low-order symmetrical $z$-IO/$\rho$-PR mixing mode with $m = 0$ is stressed by the symbol "$\times$." The frequency point of $\omega = 490$ cm$^{-1}$ is just consistent with the recent experimental observation of interface optical phonon modes in ZnO QDs [35]. Due to the lowest-order phonon mode ($n = 1$) and the spherical symmetry of phonon potential ($m = 0$), we suggest that the phonon modes ($\omega$=490 cm$^{-1}$) observed in ZnO QDs experiments [35] are the symmetrical $z$-IO/$\rho$-PR mixing phonon modes with $m = 0$. Same as the situation of $\rho$-IO/$z$-PR mixing phonon modes (Figure 1), the dispersive frequencies of $z$-IO/$\rho$-PR mixing modes are also the discrete functions of $k_{z1}$. The dispersive frequencies of the high (low) frequency $z$-IO/$\rho$-PR mixing modes are the monotonic and degressive (incremental) functions

of $k_{z1}$. As $k_{z1}$ approaches infinity, the two branches of $z$-IO/$\rho$-PR mixing modes converge to the frequency of 558.5 cm$^{-1}$. This limiting value is determined by the relation $\epsilon_{z1}+1=0$. In fact, with the aid of the limiting relations of Bessel function and Neumann function (20) [43]

$$\begin{aligned}\lim_{x\to\infty} J_m(x) &= \sqrt{\frac{2}{\pi x}}\cos\left[x-(m+\frac{1}{2})\right]\frac{\pi}{2},\\ \lim_{x\to\infty} Y_m(x) &= \sqrt{\frac{2}{\pi x}}\sin\left[x-(m+\frac{1}{2})\right]\frac{\pi}{2},\end{aligned} \tag{20}$$

as $k_{z1}\to\infty$, the equation (8) can reduce naturally to the form of $\epsilon_{z1}+1=0$. This explains distinctly the mathematic origin of the limiting frequency values of 558.5 cm$^{-1}$ for very large wave-number $k_{z1}$. Moreover, the equation $\epsilon_{z1}+1=0$ also determines the dispersive frequency of $z$-direction IO phonon modes in wurtzite planar heterostructure [24, 25, 26, 29, 30, 31]. From a physical viewpoint, the wave-lengths of phonon modes become very short as $k_z\to\infty$, thus the phonons cannot distinguish planar heterostructure and the curved cylindrical heterostructure [44]. This directly results in the identical limiting frequency of phonon modes in wurtzite planar heterostructure and QD systems for very large wave-numbers [24, 25, 26, 29, 30, 31]. Compared the symmetrical $z$-IO/$\rho$-PR mixing modes with the antisymmetrical $z$-IO/$\rho$-PR mixing modes, it is found that the dispersions of the symmetrical modes are more obvious than those of the antisymmetrical modes. As $m$ is fixing, the intervals of adjacent $k_{z1}$ are unequal. The intervals decrease with the increase of $k_{z1}$, which differ obviously from the cases of $\rho$-IO/$z$-PR mixing modes (refer to Figure 1). The larger the azimuthal quantum number $m$, the smaller the adjacent intervals of $k_{z1}$ become. We note that the antisymmetrical $z$-IO/$\rho$-PR mixing modes occur at $k_{z1}>0.3$ nm$^{-1}$, which is the typical reducing behaviors of confined phonon modes in anisotropic wurtzite quantum structures. In fact, as $\omega$ is over than $\omega_{tL1}$, the sign of $\epsilon_{t1}(\omega)\epsilon_{z1}(\omega)$ will become negative, thus the old IO-PR mixing phonon modes cannot exist in this situation, and they will reduce to the other phonon modes, such as the half-space modes or quasi-confined modes [24, 25, 26, 27, 28, 29, 30, 31, 32].

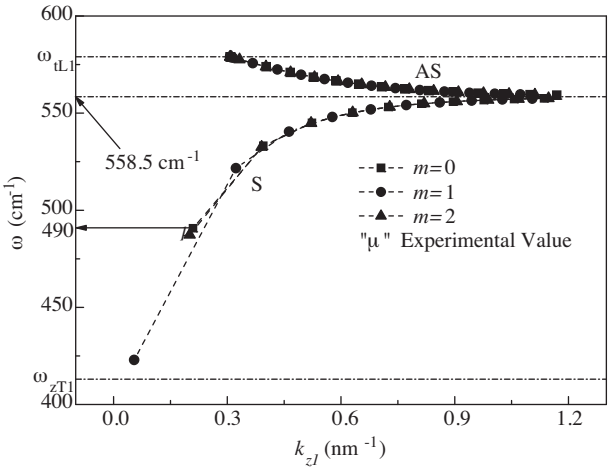


**Figure 2**. Dispersive frequencies $\omega$ of the $z-$IO/$\rho-$PR mixing modes as a function of $k_{z1}$ for three different azimuthal quantum numbers $m=0,1,2$. The symbol "$\times$" in the figure denotes the experiment frequency of interface optical phonon modes in wurtzite ZnO QDs [35].

On the other hand, it is found that the wave-number $k_{z1}$ becomes continuous as $d \to \infty$ from equations (5) or (7). Under this condition, based on equation (3) one can get the relations:

$$\begin{aligned} k_{z1} &= k_{z2} = k_z, \\ k_{ti} &= \sqrt{\epsilon_{zi}(\omega)/\epsilon_{ti}(\omega)}k_z. \end{aligned} \tag{21}$$

Substituting the two conditions of equation (21) into the equations (6) and (8), equation (6) will reduce to the form of dispersive equation which is completely same as the dispersive equation of IO phonon modes in Q1D wurtzite QWRs [31], and the equation (8) will reduce to the dispersive equation of the PR modes in Q1D wurtzite QWRs [32]. This explains distinctly the fact, from a mathematical view of point, that the IO-PR mixing phonon modes in Q0D wurtzite QDs reduce to the IO or PR phonon modes in Q1D wurtzite QWRs under the condition of $d \to \infty$. From a pure physical viewpoint, as the height $d$ approaches $\infty$ and the radius $R$ is kept at a finite value, the physical model of the wurtzite Q0D cylindrical QD structures will naturally reduce to the wurtzite Q1D cylindrical QWR structures. In the same way, as the height $d$ takes a certain value and the radius $R$ approaches infinity, via the limiting relations (20), the wave-number $k_{ti}$ $(i = 1, 2)$ will become continual based on equations (6) or (8). From equations (3), one can get the relations

$$\begin{aligned} k_{t1} &= k_{t2} = k_t \\ k_{zi} &= \sqrt{\epsilon_{ti}(\omega)/\epsilon_{zi}(\omega)}k_t. \end{aligned} \tag{22}$$

Thus equation (7) [equation (5)] reduces to the dispersive equation of IO (PR) phonon modes in Q2D wurtzite QWs. This mathematical result illustrates clearly that, when $R \to \infty$, the $z$-IO/$\rho$-PR mixing modes will reduce to the IO and PR modes in Q2D wurtzite QWs. These are also natural results because the cylindrical QDs will degenerate into Q2D QWs when the radius of the QDs approaches $\infty$. This further proves the correctness and reliability of the phonon modes theories in Q0D wurtzite QD systems established in the present work.

Next we discuss the characteristics of electron-phonon coupling functions in the wurtzite QDs. The coupling functions $\Gamma^{\mathrm{IO-PR}}_{m,k_{z1}}(z)$ and $\Gamma^{\mathrm{IO-PR}}_{m,k_{z1}}(\rho)$ of electron with $\rho$-IO/$z$-PR mixing phonon modes as functions of $z$ and $\rho$ are depicted in Figure 3 for the first two branches of $\rho$-IO/$z$-PR mixing modes $(n = 1, 2)$ with two azimuthal quantum numbers $(m = 0, 1)$. Figures 3(a)–(c) display the coupling properties of electron-($\rho$-IO/$z$-PR) phonon interaction in $z$-direction, and Figure 3(d) presents those in $t$-direction. The solid (dash) curves in Figures 3(a)–(c) correspond the antisymmetrical (symmetrical) electron-($\rho$-IO/$z$-PR) phonons coupling functions. And the curves in Figure 3(d) display the coupling properties of electron-($\rho$-IO/$z$-PR) phonons interaction in $t$-direction with different phonon branches $(n = 1, 2)$ and azimuthal quantum numbers $(m = 0, 1)$. From the figures, we observed that, for certain $m$ and $n$, there are two oscillating waves in $z$-direction. One is symmetrical, and the other is antisymmetrical. The coupling functions $\Gamma^{\mathrm{IO-PR}}_{m,k_{z1}}(\rho)$ (Figure 3(d)) take their maximum values at the side interface $\rho = a_B$, and decrease from both sides of the interface. Based on the oscillating (decreasing) feature in $t$-($z$-) direction, these phonon modes are labeled by $\rho$-IO/$z$-PR mixing phonon modes. Comparing Figure 3(a) with (b), one can find that the coupling strength of $\Gamma^{\mathrm{IO-PR}}_{m,k_{z1}}(z)$ has obviously increase with the increase of $n$. It is found from Figures 3(a) and (c) that, $\Gamma^{\mathrm{IO-PR}}_{m,k_{z1}}(z)$ nearly keeps unchanged as azimuthal quantum number $m$ increases for a fixed $n$. From Figure 3(d), it is seen clearly that the coupling strengths of $\Gamma^{\mathrm{IO-PR}}_{m,k_{z1}}(\rho)$ between electron with $\rho$-IO/$z$-PR mixing modes in $t$-direction have

distinctly increase as $m$ or $n$ increases. This obviously differs from the situations of electron-phonon coupling functions in cubic GaAs-based low-dimensional quantum structures [15, 20, 45]. In cubic GaAs-based quantum systems, the electron-phonon coupling strength decreases with the increase of azimuthal quantum number and order of phonon modes. The reason resulting in the difference in the two systems (ZnO and GaAs-based systems) mainly lies in the fact of their different crystal structures, i.e. GaAs-based crystals are zinc-blende structures, and ZnO crystal is anisotropic wurtzite structure.

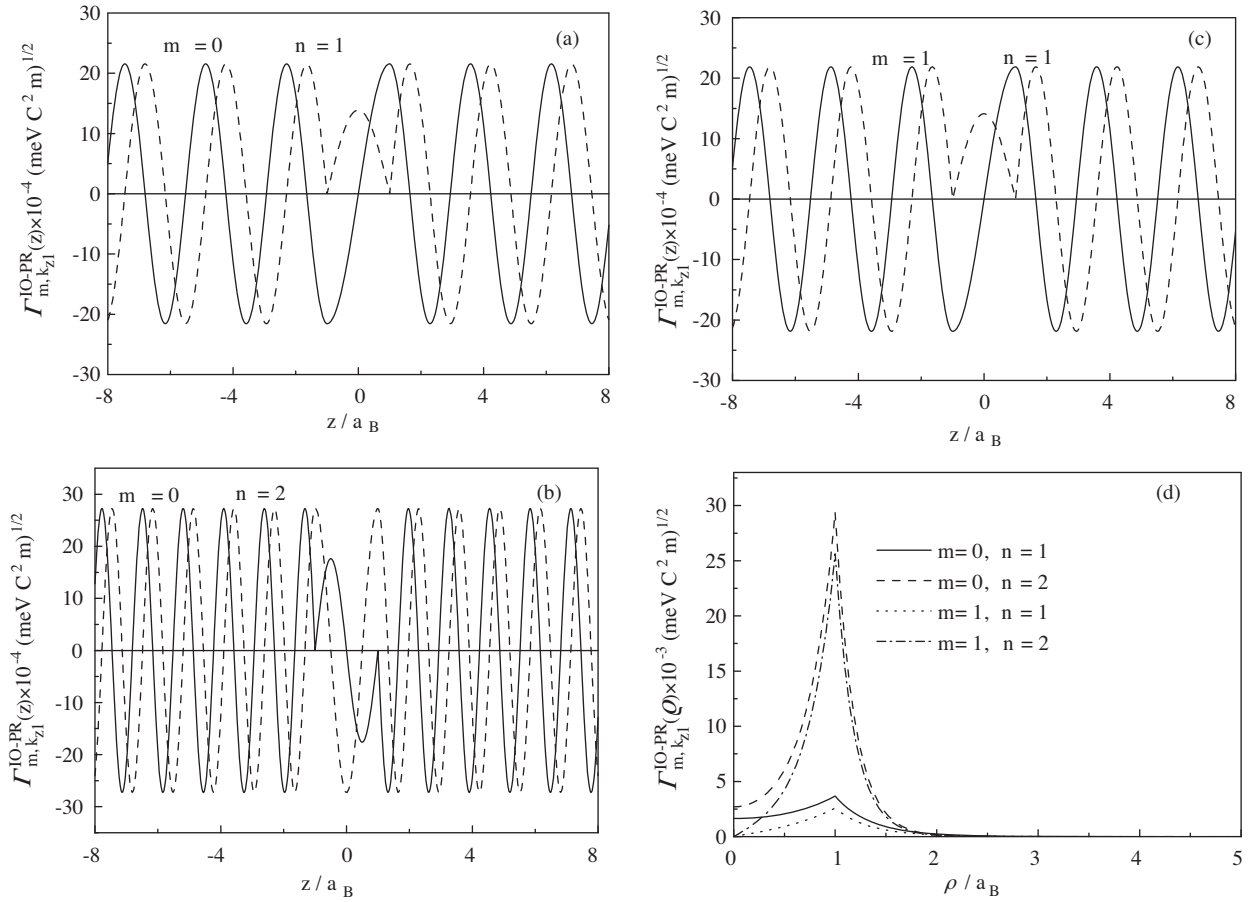


**Figure 3**. Coupling functions $\Gamma^{\mathrm{IO-PR}}_{m,k_{z1}}(z,\rho)$ of electron with $\rho$-IO/$z$-PR mixing phonon modes as functions of $z$ and $\rho$ for the first two branches of $\rho$-IO/$z$-PR mixing modes ($n = 1, 2$) with two azimuthal quantum numbers ($m = 0, 1$). The solid (dash) curves in Figure (a)-(c) correspond the antisymmetrical (symmetrical) electron-($\rho$-IO/$z$-PR) phonons coupling function. And the curves in Figure (d) denote the coupling functions of electron-($\rho$-IO/$z$-PR) phonons interaction in $t$-direction with different phonon branches ($n = 1, 2$) and azimuthal quantum numbers ($m = 0, 1$).

The coupling functions $\Gamma^{\mathrm{IO-PR}}_{m,k_{z1}}(\rho,z)$ of electron with antisymmetrical $z$-IO/$\rho$-PR mixing phonon modes as functions of $z$ and $\rho$ are plotted in Figure 4. For clarity, only the first six branches of antisymmetrical $z$-IO/$\rho$-PR mixing modes are depicted, and two azimuthal quantum numbers $m = 0$ [Figures 4(a) and (b)], 1 [Figures 4(c) and (d)] are chosen. The distributions of coupling functions $\Gamma^{\mathrm{IO-PR}}_{m,k_{z1}}(z)$ in $z$-direction are decaying and antisymmetrical (Figures 4(a) and (c)), while those of coupling functions $\Gamma^{\mathrm{IO-PR}}_{m,k_{z1}}(\rho)$ in $t$-direction

are vibrational. This is just the reason why these phonon modes are labeled by antisymmetrical $z$-IO/$\rho$-PR mixing phonon modes. In Figures 4(a) and (c), the electron-phonon couplings $|\Gamma^{\mathrm{IO-PR}}_{m,k_{z1}}(z)|$ of $n = 4$ mode are the strongest relative to those with $n = 1, 2, 3, 5, 6$. In Figure 4(b) [(d)], the electron-phonon couplings $|\Gamma^{\mathrm{IO-PR}}_{m,k_{z1}}(\rho)|$ of $n = 3\,[n = 1]$ modes is stronger in contrast to the other modes. In fact, when $m$ and $n$ are over than 10, the coupling functions $\Gamma^{\mathrm{IO-PR}}_{m,k_{z1}}(\rho, z)$ decrease with the increase of $m$ and $n$ (not display here). As $m$ and $n$ are relatively small, the modulation effect of different dielectric functions in $z$- and $t$-directions plays important role on the electron-phonon coupling strength, and it leads to the abnormal increase of electron-phonon coupling strength in wurtzite quantum heterostructures. This feature has been observed in wurtzite nitride Q2D QW and Q1D QWR structures [26, 31].

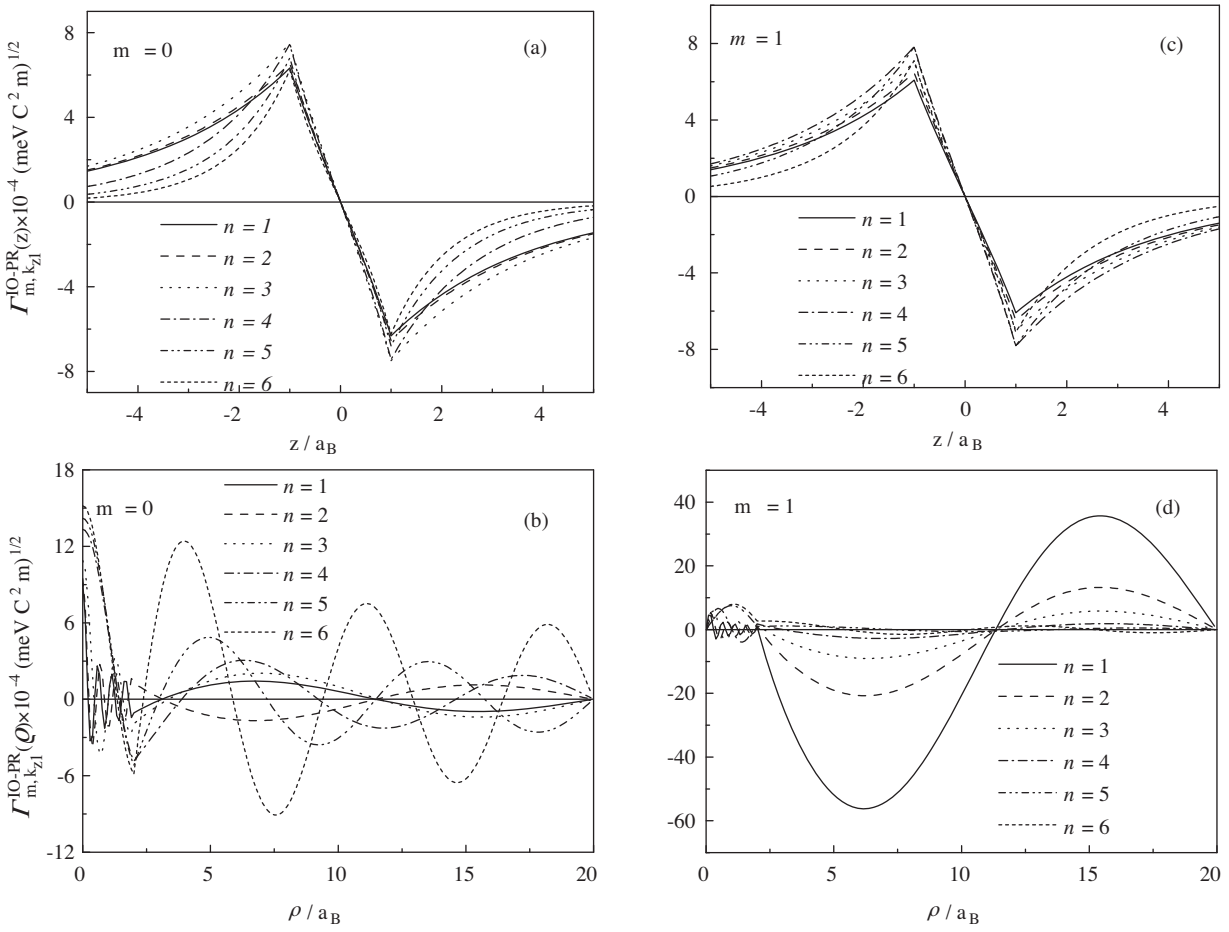


**Figure 4**. Coupling functions $\Gamma^{\mathrm{IO-PR}}_{m,k_{z1}}(z, \rho)$ of electron with antisymmetrical $z$-IO/$\rho$-PR mixing phonon modes as functions of $z$ and $\rho$ for the first six branches ($n = 1, 2, ..., 6$) of antisymmetrical $z$-IO/$\rho$-PR mixing modes with azimuthal quantum numbers $m = 0$ [(a) and (b)], 1 [(c) and (d)].

Figure 5 shows the distribution feature of the coupling functions $\Gamma^{\mathrm{IO-PR}}_{m,k_{z1}}(\rho, z)$ of electron with symmetrical $z$-IO/$\rho$-PR mixing phonon modes in $z$- and $t$- directions. Same as Figure 4, only the first six branches of symmetrical $z$-IO/$\rho$-PR mixing modes with azimuthal quantum numbers $m = 0, 1$ are displayed here for

clarity. Obviously, the coupling functions $\Gamma^{\mathrm{IO-PR}}_{m,k_{z1}}(z)$ in $z$-direction are symmetrical and decaying from both sides of the interfaces at $z = \pm d$, and those of $\Gamma^{\mathrm{IO-PR}}_{m,k_{z1}}(\rho)$ in $t$-direction are oscillating. This explains the reason that these phonon modes are named as symmetrical $z$-IO/$\rho$-PR mixing phonon modes. For a certain $m$, the total tendency of coupling functions $\Gamma^{\mathrm{IO-PR}}_{m,k_{z1}}(\rho, z)$ decrease as $n$ increases. Moreover, a comparison of the phonon branches of Figures 5(a) and (b) with the phonon branches of Figures 5(c) and (d) show that the electron-phonon coupling strength will become weaker and weaker as $m$ increases. This feature is distinctly different from the cases of Figure 3 and Figure 4, and is completely same as the cases of electron-phonon coupling properties in GaAs-based quantum structures [15, 20, 45].

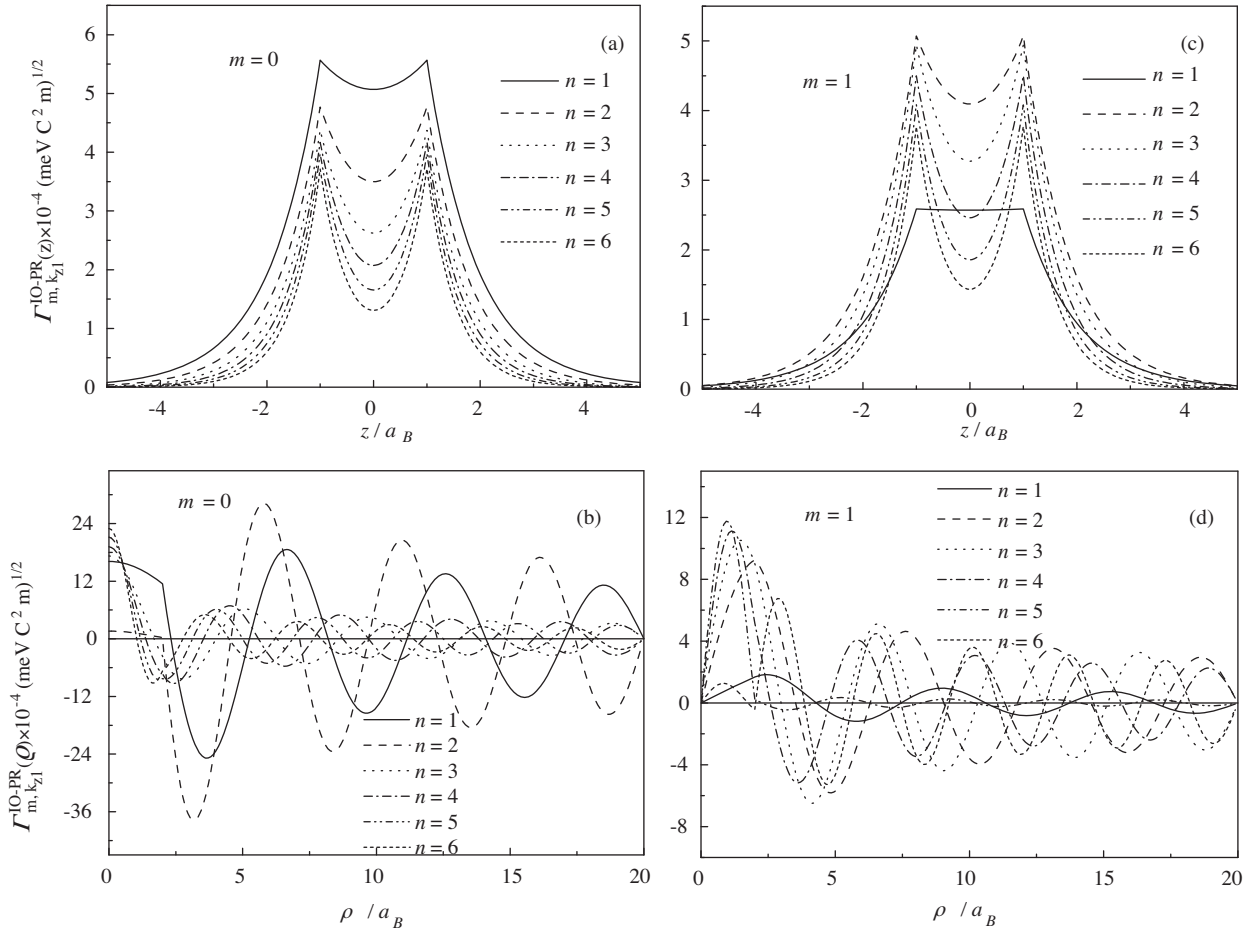


**Figure 5**. Coupling functions $\Gamma^{\mathrm{IO-PR}}_{m,k_{z1}}(\rho, z)$ of electron with symmetrical $z$-IO/$\rho$-PR mixing phonon modes as functions of $z$ and $t$ for the first six branches ($n = 1, 2, ..., 6$) of symmetrical $z$-IO/$\rho$-PR mixing modes with azimuthal quantum numbers $m = 0$[(a) and (b)], 1 [(c) and (d)].

# 4. Conclusions

In the present work, important polar-optical phonon modes, i.e. the IO-PR mixing phonon modes and their coupling behaviors with electrons in a wurtzite cylindrical QD system, have been investigated by means of the DCM and Loudon's uniaxial crystal model. It is found that there are two types of IO-PR mixing phonon modes in wurtzite cylindrical QD structures, namely the $\rho$-IO/$z$-PR mixing modes and the $z$-IO/$\rho$-PR mixing modes. Each of the IO-PR mixing phonon modes also have two forms: symmetrical and antisymmetrical. The Fröhlich-like Hamiltonian of electron-(IO-PR) mixing phonons interactions is deduced. Numerical results on a wurtzite ZnO cylindrical QD reveal that both the dispersive spectra of $\rho$-IO/$z$-PR mixing modes and $z$-IO/$\rho$-PR mixing modes can only assume a series of discrete values due to the three-dimension confinement of the QD structures. The calculated dispersive frequency supports the recent experimental result in ZnO QDs [35]. As the height or radius of the Q0D wurtzite cylindrical QDs approach infinity, both types of the IO-PR mixing modes reduce to the IO modes or PR modes in Q2D wurtzite QW and Q1D QWR structures. This shows the present theories of mixing phonon modes in wurtzite Q0D QDs are consistent with those in wurtzite Q2D QW and Q1D QWR systems [24, 25, 26, 27, 28, 29, 30, 31, 32], which further confirms the validity and reliability of phonon mode theories in wurtzite QD systems. An abnormal electron-phonon coupling strength is observed as the azimuthal quantum number and order of phonon modes increase. This is ascribed to the the modulation effect of different dielectric functions in $z$- and $t$-directions of anisotropic wurtzite ZnO material [26, 31].

We hope that the present work will stimulate further theoretical and experimental investigations of lattice dynamical properties, as well as device applications based on wurtzite ZnO QD systems.

# Acknowledgments

This work was jointly supported by NNSF under Grant No. 60906042 and Project of Yangcheng Scholar under Grant No. 10B010D, P. R. China. The author would like to acknowledge the valuable guidance and discussion of Prof. J. J. Shi of Peking University.

# Appendix

The coupling coefficients $\mathcal{B}_2$ and $\mathcal{B}_3$ [in equation (14)] of the symmetrical and antisymmetrical $\rho$-IO/$z$-PR mixing phonon modes are complex quantities. Thus they can be written as

$$\mathcal{B}_i = B_{\mathrm{R}i} + \mathrm{i}B_{\mathrm{I}i}, (i = 2, 3), \tag{23}$$

where the real quantities $B_{\mathrm{R}i}$ and $B_{\mathrm{I}i}$ denote the real part and imaginary part of $\mathcal{B}_i$, respectively. The coupling coefficients $\mathcal{B}_2$ is given by

$$B_{\mathrm{R}2} = 2k_{z2}\epsilon_{z2}\cos(k_{z1}d)\sin^2(k_{z1}d)(k_{z2}^2\epsilon_{z2}^2 - k_{z1}^2\epsilon_{z1}^2)/\mathcal{D}, \tag{24}$$

and

$$B_{\mathrm{I}2} = -2k_{z1}k_{z2}^2\epsilon_{z2}^2\epsilon_{z1}\cos(2k_{z1}d)\sin(k_{z1}d)/\mathcal{D}. \tag{25}$$

The coefficients $\mathcal{B}_3$ are given by

$$B_{\mathrm{R}3} = k_{z2}\epsilon_{z2}\sin(k_{z1}d)[k_{z2}^2\epsilon_{z2}^2 - k_{z1}^2\epsilon_{z1}^2 + \cos(2k_{z1}d)(k_{z2}^2\epsilon_{z2}^2 + k_{z1}^2\epsilon_{z1}^2)]/\mathcal{D}, \tag{26}$$

and

$$B_{\mathrm{I}3} = 0. \tag{27}$$

In equations (24)–(27), $\mathcal{D}$ is defined as

$$\begin{aligned} \mathcal{D} &= k_{z1}k_{z2}\epsilon_{z1}\epsilon_{z2}[\sin(k_{z1}d) - \sin(3k_{z1}d)] \\ &\quad \times[k_{z1}\epsilon_{z1}\cos(k_{z2}d)\sin(k_{z1}d) - k_{z2}\epsilon_{z2}\cos(k_{z1}d)\sin(k_{z2}d)]. \end{aligned} \tag{28}$$

# References


[1] Ü. Özgür, I. Alivov, C. Liu, A. Teke, M. A. Reshchikov, S. Doğan, C. Avrutin, S.-J. Cho and H. Morkoç, *J. Appl. Phys.*, **98**, (2005), 041301.

[2] Z. L. Wang, *Materialtoday*, **10**, (2007), 20.

[3] A. D. Yoffe, *Adv. Phys.*, **50**, (2000), 208.

[4] A. Nakamura, K. Okamatsu, T. Tawara, H. Gotoh, J. Temmyo and Y. Matsui, Japan. *J. Appl. Phys.*, **47**, (2008), 3007.

[5] Y. J. Zeng, Z. Z. Ye, F. Liu, D. Y. Li, Y. F. Lu, W. Jaeger, H. P. He, L. P. Zhu, J. Y. Huang and B. H. Zhao, *Crystal Growth & Design* **9**, (2009), 263.

[6] G. Mayer, M. Fonin, U. Rüdiger, R. Schneider, D. Gerthsen, N. Jan$\beta$en and R. Bratschitsch, *Nanotechnology*, **20**, (2009), 075601.

[7] Z. Z. Ye, Y. J. Zeng, Y. F. Yu, S. S. Lin, L. Sun, L. P. Zhu and B. H. Zhao, *Appl. Phys. Lett.*, **91**, (2007), 112110.

[8] L. G. Lu, Z. Z. Ye, J. Y. Huang, L. P. Zhu, B. H. Zhao, Z. L. Wang and Sz. Fujita, *Appl. Phys. Lett.*, **88**, (2006), 063110.

[9] V. A. Fonoberov, K. A. Alim, A. A. Balandin, F. Xiu and J. Liu, *Phys. Rev.*, **B73**, (2006), 165317.

[10] K. F. Lin and W.-F. Hsieh, *J. Phys. D: Appl. Phys.*, **41**, (2008), 215307.

[11] W. K. Liu, K. M. Whitaker, A. L. Smith, K. R. Kittilstved, B. H. Robinson and D. R. Gamelin, *Phys. Rev. Lett.*, **98**, (2007), 186804.

[12] X. B. Zhang, T. Taliercio, S. Kolliakos and P. Lefebvre, *J. Phys.: Condens. Matter*, **13**, (2001), 7053.

[13] K. Sood, J. Menendez, M. Cardona and K. Ploog, Phys. Rev., **B54**, (1985), 2111; **54**, (1985), 2115.

[14] A. Tanaka, S. Onari and T. Arai, *Phys. Rev.*, **B45**, (1992), 6587; **47**, (1993), 1237.

[15] H. J. Xie, C. Y. Chen and B. K. Ma, *Phys. Rev.*, **B61**, (2000), 4827.

[16] L. T. Tan, R. W. Martin, K. P. O'Donnell and I. M. Watson, *Appl. Phys. Lett.*, **89**, (2006), 101910.

[17] M. Smith, J. Y. Lin, H. X. Jiang, A. Khan, Q. Chen, A. Salvador, A. Botchkarev, W. Kim and H. Morkoc, *Appl. Phys. Lett.*, **70**, (1997), 2882.

[18] J. Cui and J. Shi, *Solid State Commun.*, **145**,(2008), 235.

[19] L. Zhang, J. J. Shi and S. Gao, *Semicond. Sci. Technol.*, **23**, (2008), 045014.

[20] L. Zhang, H. J. Xie and C. Y. Chen, *Phys. Rev.*, **B66**, (2002), 205326.

[21] W. S. Li, and C. Y. Chen, *Physica B*, **229**, (1997), 375.

[22] C. Kanyinda-Malu and R. M. de la Cruz, *Phys. Rev.*, **B59**, (1999), 1621.

[23] C. Y. Chen, W. S. Li and Ho-Kee Yeung, *Solid State Commun.*, **106**, (1998), 465.

[24] B. C. Lee, K. M. Kim, M. A. Stroscio and M. Dutta, *Phys. Rev.*, **B58**, (1998), 4860.

[25] J. Gleize, J. Frandon, F. Demangeot, M. A. Renucci, M. Kuball, J. M. Hayes, F. Widmann and B. Daudin, *Mater. Sci. Eng.*, **B82**, (2001), 27.

[26] J. Shi, *Phys. Rev.*, **B68**, (2003), 165335.

[27] J. J. Shi, X. L. Chu and E. M. Goldys, *Phys. Rev.*, **B70**, (2004), 115318.

[28] J. T. Lü and J. C. Cao, *Appl. Phys. Lett.*, **88**,(2006), 061119.

[29] L. Zhang, J. J. Shi and T. L. Tansley, *Phys. Rev.*, **B71**, (2005), 245324.

[30] L. Zhang, *Turk. J. Phys.*, **31**, (2007), 85.

[31] L. Zhang and J. J. Shi, *Commun. Theor. Phys.*, **45**, (2006), 935.

[32] L. Zhang and J. S. Liao, *Superlatt. Microstruc.*, **43**, (2008) 28.

[33] M. Rajalakshmi, A. K. Arora, B. S. Bendre and S.Mahamuni, *J. Appl. Phys.*, **87**, (2000), 2445.

[34] K. F. Lin, H.-M. Cheng, H.-C. Hsu, and W.-F. Hsieh, *Appl. Phys. Lett.*, **88**, (2006), 263117.

[35] P. M. Chassaing, F. Demangeot, V. Paillard, A. Zwick, N. Combe, C. Pages, M.L. Kahn, A. Maisonnat and B. Chaudret, *Phys. Rev.*, **B77**, (2008), 153306.

[36] P. M. Chassaing, F. Demangeot, N. Combe, L. Saint-Macary, M. L. Kahn and B. Chaudret, *Phys. Rev.*, **B79**, (2009), 155314.

[37] H. M. Cheng, K.-F. Lin, H.-C. Hsu and W.-F. Hsieh, *Appl. Phys. Lett.*, **88**, (2006), 261909; H. M. Cheng, K.-F. Lin, H.-C. Hsu, C.-J. Lin, L.-J. Lin and W.-F. Hsieh, *J. Phys. Chem.*, **B109**, (2005), 18385.

[38] W.-T. Hsu, K.-F. Lin, and W.-F. Hsieh, *Appl. Phys. Lett.*, **91**, (2007), 181913.

[39] V. A. Fonoberov and A. A. Balandin, *Phys. Rev.*, **B70**, (2004), 233205.

[40] L. Zhang, J. J. Shi and H. J. Xie, *Solid State Commun.*, **140**, (2006), 549.

[41] R. Loudon, *Adv. Phys.*, **13**, (1964), 423.

[42] N. Garro, A. Cros, J. M. Llorens, A. Garcia-Cristobal, A. C. Cantarero, N. Gogneau. E. Sarigiannidou, E. Monroy and B. Daudin, *Phys. Rev.*, **B74**, (2006), 075305.

[43] D. P. Xi, *Bessel functions*, (China Higher Education Press, Beijin. 1998), P.16.

[44] R. Enderlein, *Phys. Rev.*, **B47**, (1993), 2162.

[45] J. Shi and S. H. Pan, *J. Appl. Phys.*, **80**,(1996), 3863.